Title

Comparative study of active plasma lenses in high-quality electron accelerator transport lines



Journal

Physics of Plasmas, 25(5)

ISSN

1070-664X

Authors

van Tilborg, J

Barber, SK

Benedetti, C

et al.

Publication Date

2018-05-01

DOI

10.1063/1.5018001

# Comparative study of active plasma lenses in high-quality electron accelerator transport lines

J. van Tilborg, S. K. Barber, C. Benedetti, C. B. Schroeder, F. Isono, H.-E. Tsai, C. G. R. Geddes, and W. P. Leemans

Citation: Physics of Plasmas **25**, 056702 (2018); doi: 10.1063/1.5018001
View online: https://doi.org/10.1063/1.5018001
View Table of Contents: http://aip.scitation.org/toc/php/25/5
Published by the American Institute of Physics

# Comparative study of active plasma lenses in high-quality electron accelerator transport lines

J. van Tilborg,[1,a),b)] S. K. Barber,[1] C. Benedetti,[1] C. B. Schroeder,[1] F. Isono,[1,2] H.-E. Tsai,[1] C. G. R. Geddes,[1] and W. P. Leemans[1,2]
[1]*Lawrence Berkeley National Laboratory, Berkeley, California 94720, USA*
[2]*University of California, Berkeley, California 94720, USA*

(Received 2 December 2017; accepted 7 February 2018; published online 13 March 2018)

Electrically discharged active plasma lenses (APLs) are actively pursued in compact high-brightness plasma-based accelerators due to their high-gradient, tunable, and radially symmetric focusing properties. In this manuscript, the APL is experimentally compared with a conventional quadrupole triplet, highlighting the favorable reduction in the energy dependence (chromaticity) in the transport line. Through transport simulations, it is explored how the non-uniform radial discharge current distribution leads to beam-integrated emittance degradation and a charge density reduction at focus. However, positioning an aperture at the APL entrance will significantly reduce emittance degradation without additional loss of charge in the high-quality core of the beam. An analytical model is presented that estimates the emittance degradation from a short beam driving a longitudinally varying wakefield in the APL. Optimizing laser plasma accelerator operation is discussed where emittance degradation from the non-uniform discharge current (favoring small beams inside the APL) and wakefield effects (favoring larger beam sizes) is minimized. *Published by AIP Publishing*. https://doi.org/10.1063/1.5018001

## I. INTRODUCTION

Laser plasma accelerators (LPAs)[1] have produced MeV to multi-GeV electron beams in mm-to-cm scale plasma structures.[2–9] The LPA community is pursuing applications such as ultra-fast electron beam pump-probe studies,[10] compact light sources including coherent X-rays[11–15] and incoherent MeV photons,[16–19] and high-energy particle colliders.[20,21] For these applications, collimation and focusing of electron beams over short, cm-scale distances is important. Similarly, plans towards the production of high-brightness electron beams in beam-driven plasma-based accelerators[22] could benefit from strong lenses as well. Based on concepts revived from the 1950s ion accelerator community,[23–26] Ref. 27 demonstrated that discharged gas-filled capillaries[28–31] have the potential to be of great value to compact accelerator applications, due to the tunability, large magnetic field gradients (>3000 T/m), and radial focusing symmetry for electron beams. Such an active plasma lens (APL) allows for cm-scale focal lengths for GeV-level electron beams.

Subsequent APL studies were performed in two parallel efforts,[32,33] highlighting the role that the non-uniformity in the radial distribution of the discharge current plays. Dominated by a radially varying plasma temperature $T_e$[34] (warmer on-axis and cooler near the walls), the plasma resistivity [and thus the discharge current distribution $J(r)$] follows a $J(r) \sim T_e^{3/2}(r)$ scaling. An analytical expression for $J(r)$ was derived in Ref. 32, together with the radial dependence on the azimuthal focusing field $B(r)$. The non-linear component of $B(r)$ results in potential emittance degradation which places limits on the applicability of APLs, depending on the input beam parameters and desired beam quality constraints. While previous work[33] has reported on the emittance degradation from the non-linear $B(r)$, here we address several other relevant beam parameters such as the beam size and charge density at the focal plane.

A second consideration is the detrimental role of beam-driven wakefields in the APL, where the electrons in the tail of the beam are affected by the self-driven plasma wave.[1] A longitudinally varying focusing force (in addition to the discharge current's focusing force) can lead to emittance degradation. While the high charge density and low emittance may appear to make this effect problematic to high-brightness beams, the ultra-short bunch duration in LPAs combined with low APL plasma densities is favorable towards mitigating the emittance degradation. Inclusion of wakefield effects to APL considerations was not presented before.

This paper is organized as follows: Sec. II presents experimental results on energy-dispersed beam size measurements directly comparing a permanent-magnet quadrupole (PMQ) triplet with the active plasma lens (APL). Such a direct comparison under similar transport conditions, highlighting the favorable reduction in the chromatic dependence for the APL, has not been reported yet. Two critical transport considerations will be discussed in the following two sections: Sec. III presents transport modeling giving insight into the role of the non-linear discharge current, while Sec. IV derives an analytical expression for emittance degradation from beam-driven wakefields inside the APL. An example transport lay-out balancing both degradation effects is discussed in Sec. V, followed by a conclusion section.

Note: Paper YI3 2, Bull. Am. Phys. Soc. **62**, 405 (2017).
[a)]Invited speaker.
[b)]JvanTilborg@lbl.gov

## II. EXPERIMENTAL COMPARISON OF APL WITH A QUADRUPOLE TRIPLET

In order to compare the transport characteristics of the APL directly with those of a PMQ triplet, the triplet in the experimental setup described in Ref. 35 was replaced by an APL of length $L_{APL} = 1.5$ cm and radius $R_{APL} = 500\ \mu$m, see the schematic in Fig. 1. The comparative experiment was carried out at LBNL's BELLA Center using the TREX Ti:sapphire laser which delivered 1.8 J pulses of 45 fs duration that were focused by a 2 m focal length off-axis parabola to spot sizes of $w_0 = 22\ \mu$m. The LPA target consisted of a supersonic helium gas jet with a diameter of 840 $\mu$m.[36] A thin blade with an adjustable position impinged the gas flow to provide the necessary sharp density transition, allowing for density downramp injection and acceleration[37–41] and enabling precise tunability of the central energy of the electron beams (from <40 MeV to >200 MeV) by adjusting the effective accelerator length.[36] The LPA plasma profile can be described to have a length of 2 mm and a peak density of $6 \times 10^{18}$ cm$^{-3}$, with a sharp $2 \times 10^{18}$ cm$^{-3}$ drop approximately halfway. The LPA was optimized to deliver stable electron beams with a central energy of 57 MeV, a central energy fluctuation of 2 MeV (rms), an energy spread of 4 MeV (rms), a pointing fluctuation of 0.5–1 mrad (rms), and integrated charge approximately 80 pC.

The 25-mm-bore PMQ triplet was discussed in Refs. 42 and 43, with [length (mm), gradient-x (T/m), gradient-y (T/m)] for the first quadrupole (39, 51.9, −51.3), thus focusing in $x$, the second quadrupole (54.5, −50.9, 51.0), and the third quadrupole (25.5, 51.3, −51.1). The first quadrupole was positioned 17 cm from the LPA source, with a 1.73 m drift from the third quadrupole exit to the magnetic spectrometer entrance. When the triplet was removed, the APL was positioned 24 cm from the LPA source. Extensive transport modeling was performed (including higher-order transport matrix elements) to characterize the details of the transport line (drifts, lenses, dipole magnet, fringe fields, etc.). It was found that for the source parameters retrieved in the experiments, the first-order matrix elements adequately described the transport parameters. This leads to the following generalized expression for the modeled electron beam size at the YAG screen in the dispersive plane:

$$\sigma_y(E) = \sqrt{[R_{34}(E^*)]^2 \left(\frac{\epsilon_{n0}}{\gamma\sigma_0}\right)^2 + [R_{33}(E^*)]^2\sigma_0^2}, \qquad (1)$$

where $E^* = E - \Delta E$ incorporates minor focused-energy shifts from fluctuations in the longitudinal source location and transport matrixes $R_{33}$ and $R_{34}$ represent the coupling of the source size and divergence to the beam size at the screen, respectively. Besides $\Delta E$, note that only the source size $\sigma_0$ and source normalized emittance $\epsilon_{n0}$ are free fitting parameters. Table I provides an overview of the matrix elements in Eq. (1) for the two lens configurations (with $E$ in MeV).

Although the experimental data in the triplet configuration were already extensively discussed in Ref. 43, a representative single-shot energy-dispersed YAG screen image is shown in Fig. 2(a). At the focused energy of 56.93 MeV, the transverse line-out is presented in (b) and the beam size versus energy $\sigma_y(E)$ in (e) as red circles. The imaging resolution

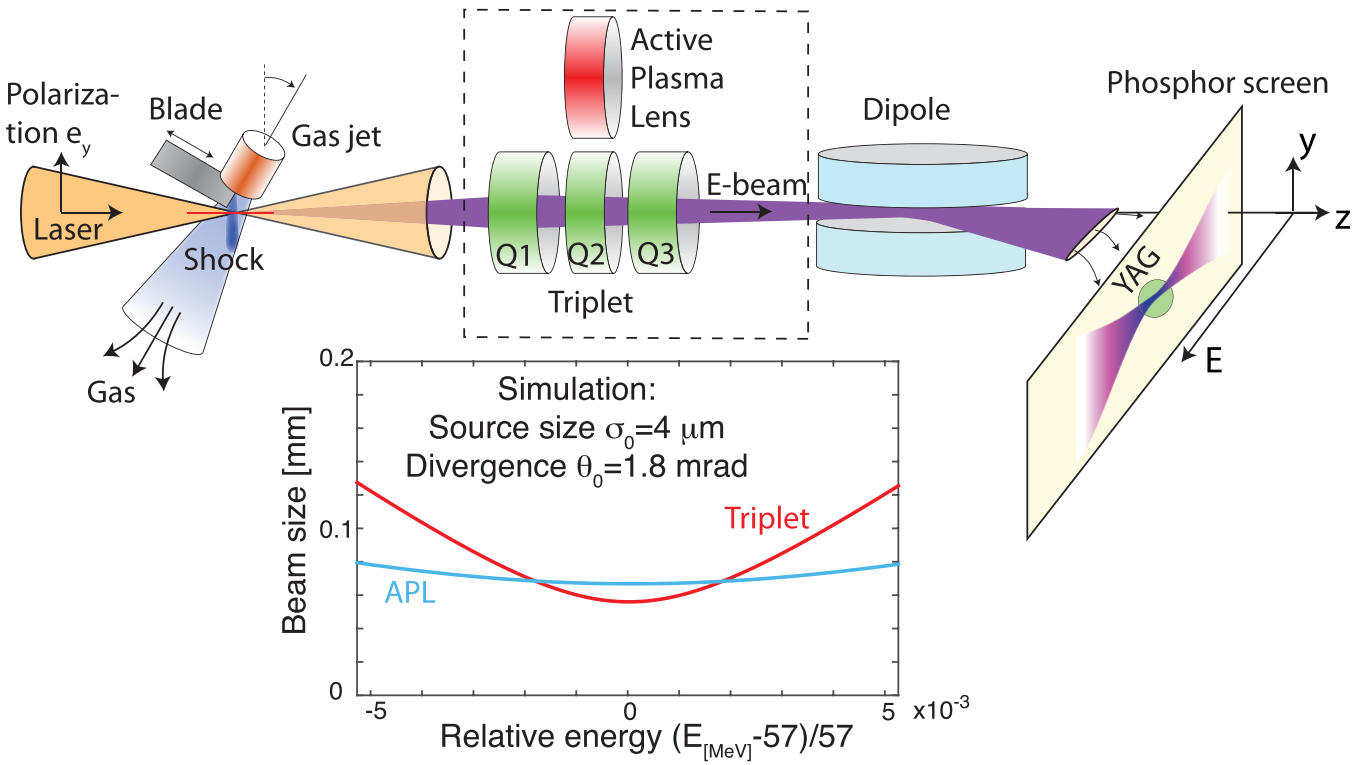


FIG. 1. Schematic of the experiment, consisting of the LPA source, a magnetic lens (either a PMQ triplet or an APL), and a YAG screen positioned at the energy-dispersed plane of a magnetic spectrometer. The inset shows the simulated energy-dispersed beam size $\sigma_y(E)$ for both lens options for the same source parameters, highlighting the reduced energy dependence (chromaticity) for the APL.

TABLE I. Transport matrix elements for triplet and APL configurations.

| Triplet |
|---|
| $R_{33} = 0.91 \times (E - 57) - 14$ |
| $R_{34} = 0.21 \times (E - 57)$ |
| **Active plasma lens** |
| $R_{33} = 0.32 \times (E - 57.3) - 16.7$ |
| $R_{34} = 0.078 \times (E - 57.3)$ |

was 8 $\mu$m, and the energy resolution was well below 0.1%. Note that $\sigma_y$ was obtained by fitting the transverse line-out above the half-of-peak threshold [thus within the full width at half maximum (FWHM)], yielding a Gaussian fit of form $\sim \exp[-y^2/(2\sigma_y^2)]$ with rms size $\sigma_y$. For $\sigma_0 = 4\,\mu$m and $\theta_0 = 2.4$ mrad (thus a normalized source emittance of $\epsilon_{n0} = 1.0\,\mu$m), an excellent match to the data was retrieved [solid red curve in Fig. 2(e)]. It is interesting to observe that the transverse beam profile in Fig. 2(b) contains wings. With the higher-order transport model, it was verified that these wings cannot be attributed to fringe fields in the quadrupoles or dispersive magnets or from coupling of the LPA divergence with energy dispersion. It is most likely that these wings either originated at the LPA source or developed through the space-charge contribution over the multi-meter propagation from the source to the YAG screen. The latter appears to be confirmed by recent space charge simulation studies.[44]

After replacing the triplet with the APL, several shots were recorded. The discharge current was approximately 55 A, and the APL plasma density was approximately $0.5 - 1 \times 10^{17}$ cm$^{-3}$. Positioned at 24 cm from the source, the limiting acceptance of the APL was approximately $\pm 2$ mrad, thus clipping the wings of the electron beam. The limiting aperture reduced the "effective" source divergence to approximately the 4 mrad $/\sqrt{8\ln 2} = 1.8$ mrad rms level and made the charge throughput more sensitive to pointing fluctuations. A representative single-shot image is shown in Fig. 2(c), with line-out in (d) and energy-dispersed beam size $\sigma_y(E)$ as blue circles in (e). The solid blue curve in (e) demonstrates the excellent agreement with the model based on $\sigma_0 = 3.8\,\mu$m and $\theta_0 = 1.8$ mrad ($\epsilon_{n0} = 0.74\,\mu$m). Two

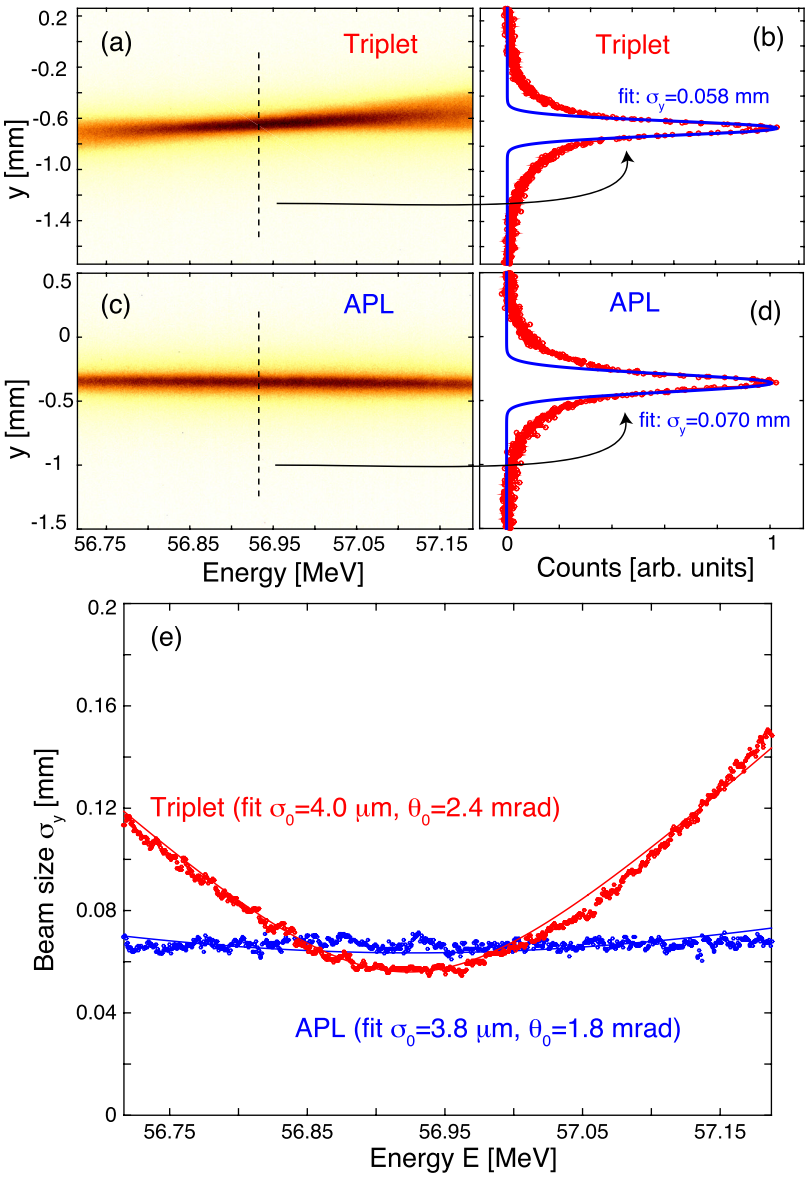


FIG. 2. Single-shot energy dispersed charge distribution in the case of the (a) PMQ triplet and (c) the active plasma lens (APL). Vertical line-outs at the optimal focused energy are shown in (b) and (d), with the solid blue line presenting a core-beam Gaussian fit yielding size $\sigma_y$. (e) shows the energy-dispersed beam size $\sigma_y(E)$, highlighting the weak energy dependence in the case of the APL. The solid lines in (e) represent the model of Eq. (1) with the source size $\sigma_0$ and source divergence $\theta_0$ as variables.

interesting observations can be made: (1) the transverse charge profiles for the APL in Fig. 2(d) and the triplet in Fig. 2(b) look similar. They both show a focused core beam with extended wings. There does not appear to be any degradation in the APL as compared to the triplet although it should be stated that APL emittance degradation as discussed in Secs. III and IV would probably not reveal itself in these experiments due to the fact that the wings are already present in the triplet case. (2) The reduced energy dependency of the APL, a consequence of the radial-symmetric focusing geometry, results in a flat profile in Fig. 2(c), compared to the triplet bow-tie profile in Fig. 2(d). This difference is evident in the steepness of the parabolic fits in Fig. 2(e). For the same source parameters, the inset in Fig. 1 highlights the same concept. The reduced chromaticity is a unique advantage of APLs [although the reduced chromaticity does require the measurement of $\sigma_y(E)$ over a larger energy bandwidth to retrieve the emittance]. Note that the triplet could have been rotated by 90° to a focusing/defocusing/focusing geometry in $y$, and although that would have reduced chromaticity in the $y$ plane, it would have equivalently increased chromaticity in the $x$ plane (which couples to the degraded energy resolution in the magnetic spectrometer).

## III. TRANSPORT SIMULATIONS WITH DISCHARGE CURRENT NON-UNIFORMITY

As was mentioned in the Introduction and outlined in Ref. 32, due to radial plasma temperature gradients in the APL, the discharge current will not be uniformly distributed. This leads to a radial dependence on the azimuthal magnetic field $B(r)$ that is no longer linear as would be desired for an ideal lens and drives an enhancement of the on-axis gradient. In the cold wall limit, the profile $B(r)$ near the axis was found to be described by $B(r) = 1.48(\partial B/\partial r)_{\rm lin} r(1 - c_n r^2)$, where $(\partial B/\partial r)_{\rm lin} = \mu_0 I_{\rm APL}/2\pi R_{\rm APL}^2$ is the uniform-current gradient, $c_n^{-1} = (56/3)u(0)^{4/7} R_{\rm APL}^2$, and $u(0) = 0.067$. Here, $\mu_0$ is the vacuum permeability. The presence of the non-linear field profile was experimentally confirmed by measurements of near-axis gradient enhancements,[32,33] the appearance of ring-shaped beams down-stream of the APL,[32] and a significant emittance degradation[33] of order $\times 10$.

Here, the results of a particle tracking simulation are presented and discussed, focusing on the role and implications of the non-linear $B(r)$ profile. 250 MeV electrons ($\gamma = 489$) are considered in a one-dimensional (1D) source-to-focus simulation. The simulation tracks $10^5$ particles distributed at the source following a Gaussian distribution with a rms size of $\sigma_0 = 1\ \mu$m and a divergence of $\theta_0 = 1$ mrad (rms) (normalized emittance $\epsilon_{n0} = 0.49\ \mu$m). These parameters were chosen to approximately match the LPA FEL design pursued in Fig. 2 of Ref. 15. Following 15 cm of drift, the beam propagated through an APL with a radius of $R_{\rm APL} = 500\ \mu$m and a length of $L_{\rm APL} = 1.5$ cm. A near-axis field gradient of $(\partial B/\partial r) = 471$ T/m ensured that the beam was focused 50 cm down-stream of the capillary exit onto a focal plane. The radial profile of the beam at the APL entrance is shown in Fig. 3(a) (dashed black curve). An ideal APL [uniform-$J(r)$, see the red curve in Fig. 3(a)] will be compared with the non-uniform-$J(r)$ case, see the blue curve based on the 3rd-order correction to $B(r)$ from Eq. (7) in Ref. 32.

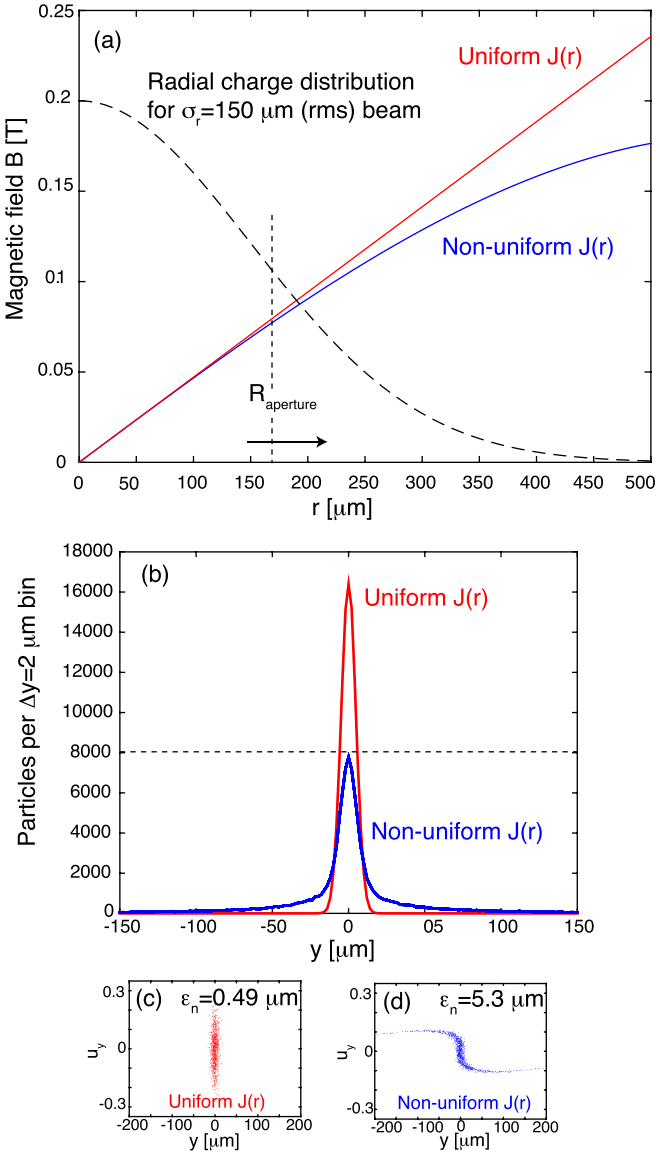


FIG. 3. (a) The focusing magnetic field dependence on radius $r$ with (blue) and without (red) discharge current uniformity (the near-axis gradient was held constant). The beam distribution at the APL entrance (from $\theta_0 = 1$ mrad divergence and 15 cm drift) is shown as the dashed black curve. At the post-APL focus, the simulated transverse charge distribution is shown for both cases in (b), with the phase space $(y, u_y)$ distribution in (c) and (d), respectively. The non-uniform $J(r)$ affects the electrons near the APL walls, resulting in wings around the focused core beam, as well as a significant emittance degradation (from $\epsilon_n = 0.49\ \mu$m to 5.3 $\mu$m).

The transverse charge distribution and phase-space $(y, u_y)$ scatter plot at focus are shown in Figs. 3(b)–3(d), for both the uniform (red) and the non-uniform $J(r)$ case (blue). Here, $u_y$ is the electron momentum normalized to $m_e c$, with $m_e$ being the electron rest mass and $c$ being the vacuum speed of light. The current non-uniformity mainly affects the electrons that propagate near the wall of the APL and leads to the development of tails or wings at focus without affecting the core beam size. The normalized rms emittance of the beam has degraded by over an order of magnitude to $\epsilon_n = 5.3\ \mu$m. However, the beam-integrated emittance degradation does not capture the

complexities of the non-ideal APL. For example, one can also observe in Fig. 3(b) that the 1D charge density is only degraded by a factor of $\times 2$, while the FWHM is approximately conserved.

In order to characterize the beam, Figs. 4(a)–4(d) present relevant aspects of the focused beam in the simulated condition of placing a limiting aperture of radius $R_{\text{aperture}}$ at the APL entrance. While in an actual beamline, the metallic aperture will not fully stop relativistic electrons at $r > R_{\text{aperture}}$, the emittance degradation of those particles will be assumed to be so dramatic that they are no longer transported well and can thus be conceptually considered to have been removed from the core beam. The black curve in Fig. 4(a) displays the 1D normalized charge throughput of the aperture (the beam has a 150 $\mu$m rms size at the APL entrance), while the red and blue curves display the normalized charge retrieved within the FWHM of the beam at final focus. For the non-uniform-$J(r)$ case (blue curve), the particles near the APL walls are deflected away from focus, and thus, removing those particles with the aperture does not affect the total charge within the focused-beam FWHM. Due to the imaging condition and the fact that the core beam in both the cases experiences the same linear focusing gradient, the beam at focus has a relatively constant FWHM independent of aperture opening, see Fig. 4(b). Figure 4(c) displays the emittance of the electron beam at focus versus aperture radius. For full opening ($R_{\text{aperture}} = 500\,\mu$m), the emittance degradation is $\times 10$, but this number is heavily dominated by the wing particles [blue outliers in Fig. 3(d)]. In other words, whether the aperture has a radius of 500 $\mu$m or 125 $\mu$m in the non-uniform-$J(r)$ case, the FWHM at focus and the charge within the FWHM are identical, but the emittance at $R_{\text{aperture}} = 125\,\mu$m is almost identical to the uniform-$J(r)$ case. For an application experiment where the beam brightness $B_{4D}$ is important [$B_{4D} \propto N_e/\epsilon_x\epsilon_y$, with $N_e$ being the number of electrons], Fig. 4(d) displays the ratio of charge within the FWHM to emittance. For aperture sizes $R_{\text{aperture}} < 125\,\mu$m, the beam brightness is unaffected by the current non-uniformity and is even slightly improved compared to the open-aperture case because the loss of particles by the limiting aperture is compensated by the emittance improvement from clipping the Gaussian wings.

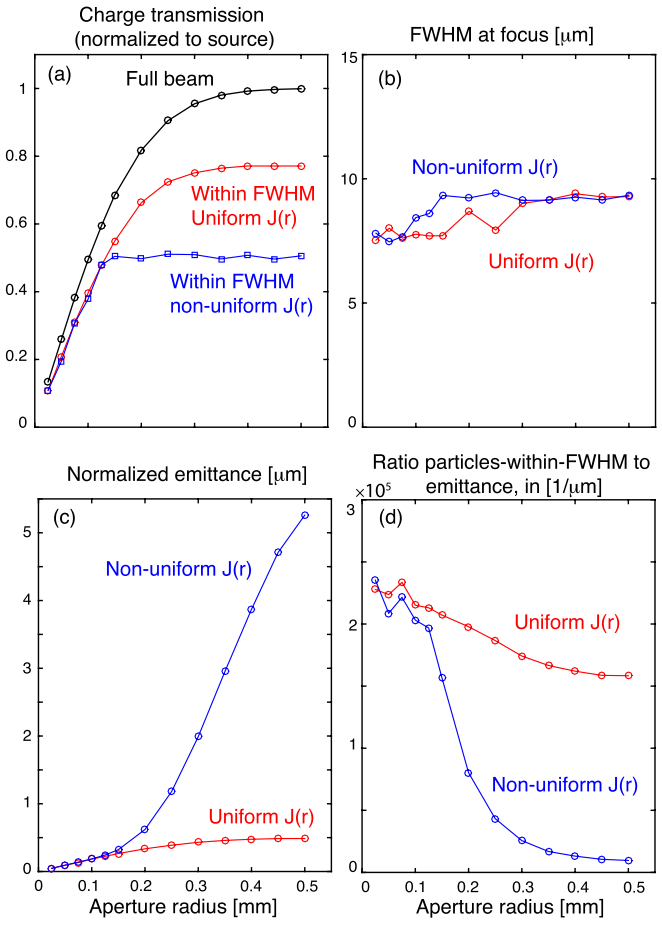


FIG. 4. Depending on the radius $R_{\text{aperture}}$ of a limiting aperture at the APL entrance, several beam parameters are analyzed in both the uniform-$J(r)$ (red) and non-uniform-$J(r)$ (blue) APL. (a) Charge in the beam normalized to the source charge (black curve) as well as the normalized charge found within the FWHM of the beam at focus for both APL cases. (b) The FWHM of the focused beam, highlighting the fact that the focused core size is fairly insensitive to aperture opening (as expected in an imaging configuration). (c) Emittance of the beam at focus, showing a large degradation when the aperture is fully open but less degradation at smaller apertures when the electrons inside the APL are restricted to linear $B(r)$ gradients. Representing a measure of the 4D beam brightness, the ratio of particles within the FWHM at focus to the emittance is plotted in (d). For smaller apertures, this ratio for a non-uniform-$J(r)$ matches the uniform-$J(r)$ case.

Although the role of the discharge current non-uniformity should be evaluated for each transport system and for each application goal, it appears that the primary consequence of the $B(r)$ non-linearity is the reduction of the effective APL radius (reduction by approximately a factor of $\times 3$ for micron-level emittances). Since the particles outside $r > R_{\text{APL}}/3$ in the APL do not contribute efficiently to the high-quality focus (and lead to emittance degradation), one can consider conceptually placing a $R_{\text{aperture}} = R_{\text{APL}}/3$ aperture at the APL entrance. For small beams at the APL entrance (rms size $\sigma_r < R_{\text{APL}}/5$), one can expect negligible charge density, emittance, and brightness degradation. For beams larger than $\sigma_r > R_{\text{APL}}/5$, the major consequence of the conceptual aperture is the loss of charge. Note that the 2D charge throughput of a $\sigma_r = R_{\text{APL}}/5$ beam through a $R_{\text{aperture}} = R_{\text{APL}}/3$ aperture is 75%.

## IV. EMITTANCE DEGRADATION FROM SELF-DRIVEN WAKEFIELDS

In this section, the role of the beam-driven wakefields inside the APL will be evaluated. In the plasma lens, the electron beam will drive a wakefield with transversally and longitudinally varying decelerating and focusing fields. Therefore, various slices of the electron beam will experience different transport conditions, which can lead to emittance growth of the integrated beam. Although contributions to emittance and energy spread degradation were derived from both the decelerating and focusing forces, for the parameters considered in this manuscript, the decelerating contribution is found to be negligible, and only the focusing contribution will be presented. The final wakefield-induced emittance growth is given in Eq. (17).

The electron beam inside the APL will be defined to have the beam density profile $n_b(\zeta, r) = n_{b0} g_{\parallel}(\zeta) g_{\perp}(r)$, with

$g_\parallel(\zeta)$ being the longitudinal profile (the bunch head is at $\zeta=0$) and $g_\perp(r)$ the radial profile, and $\zeta = z - ct$. In the linear regime, the transverse wakefield $(E_r - B_\phi)$ can be written as[1]

$$\frac{(E_r - B_\phi)}{E_0} = -\frac{n_{b0}}{n_0} S(\zeta) A(r), \tag{2}$$

with $E_0\,(\mathrm{V/m}) = 96\sqrt{n_0\,(\mathrm{cm}^{-3})}$, with $n_0$ being the APL plasma density ($k_p = 2\pi/\lambda_p$, with $\lambda_p(\mu\mathrm{m}) = 33/\sqrt{n_0(10^{18}\mathrm{cm}^{-3})}$, and $S(\zeta) = \int_{k_p\zeta}^{0} d(k_p\zeta')\, g_\parallel(\zeta') \sin k_p(\zeta - \zeta')$. The function $A(r)$ can be expressed as

$$A(r) = K_1(k_p r)\int_0^{k_p r} d(k_p r')(k_p r') I_0(k_p r') g_\perp(r') - I_1(k_p r)\int_{k_p r}^{\infty} d(k_p r')(k_p r') K_0(k_p r') g_\perp(r'), \tag{3}$$

with $I_0$ and $I_1$ being the 0th and 1st order modified Bessel functions of the first kind and $K_0$ and $K_1$ the 0th and 1st order modified Bessel functions of the second kind. Defining a flat-top longitudinal profile $g_\parallel = 1$ for $-L_b \le \zeta \le 0$ and $g_\parallel = 0$ elsewhere, it is found that within the beam

$$S(\zeta) = \cos k_p\zeta - 1 \qquad \text{for} \qquad -L_b \le \zeta \le 0. \tag{4}$$

In the limit $k_p L_b \ll 1$, the approximate expression $S(\zeta) \simeq -(k_p\zeta)^2/2$ can be used.

Here, a Gaussian form $g_\perp(r) = \exp(-r^2/2\sigma_r^2)$ for the radial beam profile will be considered, with $\sigma_r$ being the rms beam size. In the following derivation, $A(r)$ in Eq. (2) will be approximated as a linear function $A_{\mathrm{lin}}(r) = \bar{H} k_p r/2$, with $\bar{H}$ to be derived in the subsequent paragraphs. For any given value of $r$, the transverse gradient of the function $A(r)$ from Eq. (3) is approximately expressed as

$$\alpha(r) = \frac{A(r)}{k_p r}. \tag{5}$$

By averaging the expression for $\alpha(r)$ over the beam particle distribution [i.e., by weighting $\alpha(r)$ taking into account the number of particles between $r$ and $r+dr$], the following expression for the "average" slope of the function $A(r)$ in Eq. (3) is obtained

$$\langle\alpha\rangle = \frac{\int_0^\infty 2\pi r\alpha(r) g_\perp(r) dr}{\int_0^\infty 2\pi r g_\perp(r) dr} = \frac{\int_0^\infty r\left[A(r)/k_p r\right] g_\perp(r) dr}{\int_0^\infty r g_\perp(r) dr} = \frac{1}{k_p\sigma_r^2}\int_0^\infty A(r)\exp\left(-\frac{r^2}{2\sigma_r^2}\right) dr. \tag{6}$$

One can then write

$$A_{\mathrm{lin}}(r) \approx \langle\alpha\rangle k_p r \equiv \frac{\bar{H}}{2} k_p r, \tag{7}$$

where using Eq. (6)

$$\bar{H} = \frac{2}{k_p\sigma_r^2}\int_0^\infty A(r')\exp\left(-\frac{r'^2}{2\sigma_r^2}\right) dr', \tag{8}$$

with $A(r)$ expressed by Eq. (3). By performing a coordinate transformation $r' = r/k_p$ in Eq. (8), one can show that the expression $\bar{H}$ is solely a function of the normalized parameter $k_p\sigma_r$. In Fig. 5(a), the function $\bar{H} = \bar{H}(k_p\sigma_r)$ is plotted. Note that using the linear expression $A_{\mathrm{lin}}(r)$ in Eq. (2) ignores the fact that there is a small non-linear component in $A(r)$. However, the radial-weighted approximation $A_{\mathrm{lin}}$ $(r)$ allows for the calculation of the emittance degradation from the longitudinally varying focusing force.

For the transversally Gaussian beam, the quantity $n_{b0}/n_0$ can be rewritten as a function of the beam current $I_b$ as

$$\frac{n_{b0}}{n_0} = \frac{2}{(k_p\sigma_r)^2}\frac{I_b}{I_A}, \tag{9}$$

with $I_A = m_e c^3/e \simeq 17$ kA being the Alfvén current. The transverse dynamics in the horizontal ($x$) plane of a relativistic electron in an active plasma lens including wake effects is described by the following set of equations (similar equations apply in the vertical plane):

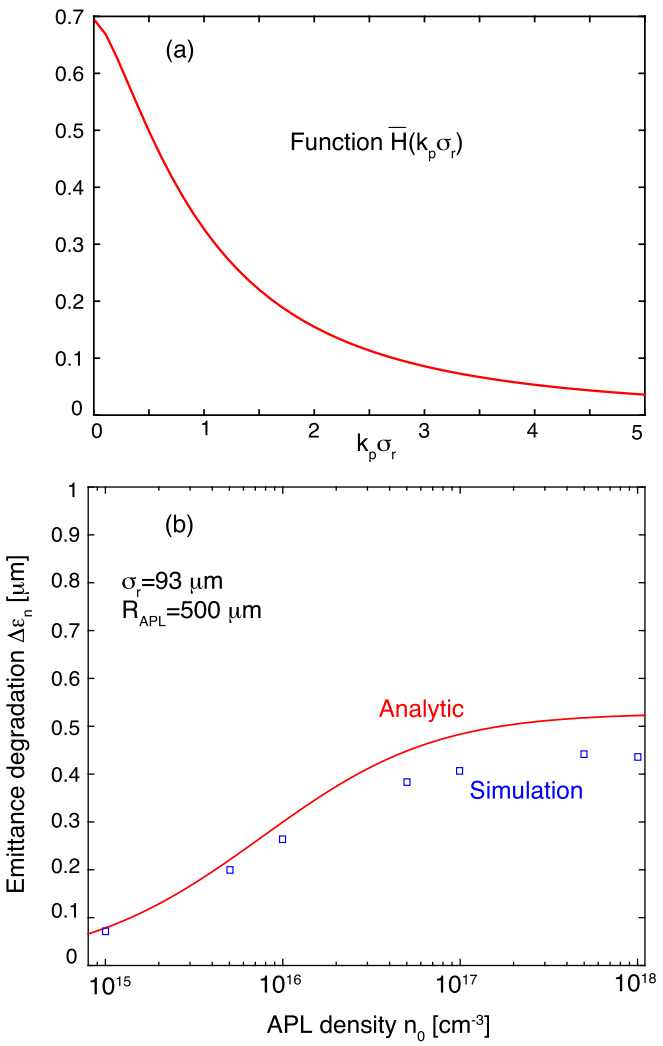


FIG. 5. (a) Function $\bar{H}(k_p\sigma_r)$. (b) Comparison of PIC simulation results (squares) versus the analytical approximate expression from Eq. (17), plotted versus APL density at electron beam parameters $\sigma_r = 93\,\mu$m, $L_b = 2\,\mu$m, and 30 pC charge. The analytical expression captures the qualitative trends (less degradation at lower APL density $n_0$), with a modest degradation overestimate of <20%.

$$\begin{cases} d(k_p x)/d(k_p s) = u_x/\gamma \\ du_x/d(k_p s) = -(k_0/k_p)^2 (k_p x) - (E_x/E_0 - B_y/E_0), \end{cases} \tag{10}$$

where $k_p x$ is the normalized transverse electron position, the term $-(k_0/k_p)^2(k_p x)$ describes the (normalized) focusing force due to the discharge current in the capillary, $\gamma$ is the particle relativistic factor, $u_x$ is the normalized transverse momentum with $u_x \ll \gamma$, $k_p s = k_p ct$ being the normalized propagation distance, $E_x$ and $B_y$ are the components of the electric and magnetic fields at the particle location, respectively. Assuming a uniform discharge current, it is found

$$\frac{k_0^2}{k_p^2} = 2\frac{I_{\mathrm{APL}}}{I_A}\frac{1}{(k_p R_{\mathrm{APL}})^2}, \tag{11}$$

where $I_{\mathrm{APL}}$ is the discharge current and $k_p R_{\mathrm{APL}}$ the normalized capillary radius. Using the approximate linear expression for the wakefield given by Eq. (7) and assuming a short longitudinal flat-top beam current profile, the equation for the electron momentum can be rewritten as

$$\begin{aligned} \frac{du_x}{d(k_p s)} &= -\frac{k_0^2}{k_p^2} k_p x - \frac{I_b}{I_A}\frac{(k_p\zeta)^2}{2}\frac{\bar{H}}{(k_p\sigma_r)^2} k_p x \\ &= -\frac{k_0^2}{k_p^2}\left[1 + \eta(k_p\zeta)^2\right] k_p x, \end{aligned} \tag{12}$$

where

$$\eta = \frac{1}{2}\frac{I_b}{I_A}\frac{\bar{H}}{(k_p\sigma_r)^2}\frac{k_p^2}{k_0^2} = \frac{1}{4}\frac{I_b}{I_{\mathrm{APL}}}\frac{(k_p R_{\mathrm{APL}})^2}{(k_p\sigma_r)^2}\bar{H}. \tag{13}$$

Equation (12) shows that the transverse force acting on an electron depends on the longitudinal location of the electron within the beam.

The APL transport line is considered to consist of a beam source, a drift of length $L_{\mathrm{drift}}$, an active plasma lens of radius $R_{\mathrm{APL}}$ and length $L_{\mathrm{APL}}$, and a final drift to focus of similar length $L_{\mathrm{drift}}$. At $\gamma$, the beam has bunch length $L_b$, source size $\sigma_0$, divergence $\theta_0$, and normalized emittance $\epsilon_{n0}$ such that $\sigma_{u_0} = \epsilon_{n0}/\sigma_0$ with $\sigma_{u_0}$ being the rms in source transverse normalized momentum. At the APL entrance, the beam size is approximately $\sigma_r \simeq \theta_0 L_{\mathrm{drift}}$. It will be assumed that there is no substantial evolution of the beam size inside the capillary. With this approximation, the effect of the APL is to change the momentum (but not the transverse position) of every particle in the beam according to Eq. (12), namely,

$$u_{x,o} = u_{x,i} - (k_0/k_p)^2\left[1 + \eta(k_p\zeta)^2\right](k_p x_i)(k_p L_{\mathrm{APL}}), \tag{14}$$

where $u_{x,i}$ and $u_{x,o}$ are the electron momentum before and after the lens, respectively, and $(k_p x_i)$ is the normalized electron transverse coordinate in the cap. One can see that the closer a particle is to the bunch tail, the larger is the transverse momentum kick it receives due to the transverse wakefield. After the second drift, at focus (i.e., $L_{\mathrm{drift}} \simeq 2\gamma/k_0^2 L_{\mathrm{APL}}$), the second order moments of the beam are

$$\begin{cases} \dfrac{\langle x^2\rangle}{\sigma_0^2} \simeq 1 + \dfrac{4}{3}\eta(k_p L_b)^2 + \dfrac{16}{5}\eta^2\dfrac{(k_p L_b)^4}{k_0^4 L_{\mathrm{APL}}^2}\dfrac{\sigma_{u_0}^2}{\sigma_0^2} \\ \langle x u_x\rangle \simeq \dfrac{4}{k_0^2 L_{\mathrm{APL}}}\left[\dfrac{1}{3}\eta(k_p L_b)^2 + \dfrac{2}{5}\eta^2(k_p L_b)^4\right]\sigma_{u_0}^2, \\ \dfrac{\langle u_x^2\rangle}{\sigma_{u_0}^2} \simeq 1 + \dfrac{4}{3}\eta(k_p L_b)^2 + \dfrac{4}{5}\eta^2(k_p L_b)^4, \end{cases} \tag{15}$$

where in the derivation, it was assumed that $(k_0/k_p)^2(k_p L_{\mathrm{APL}}) \ll 1$ (thin lens approximation). The emittance growth at focus due to wake effects is

$$\frac{\epsilon_n^2}{\epsilon_{n0}^2} \simeq 1 + \frac{64}{45}\eta^2\frac{(k_p L_b)^4}{k_0^4 L_c^2}\frac{\sigma_{u_0}^2}{\sigma_0^2}, \tag{16}$$

where the expression was simplified keeping only the dominant term. By using Eqs. (11) and (13), Eq. (16) can be rewritten as $\epsilon_n^2 = \epsilon_{n0}^2 + \Delta\epsilon_n^2$, with

$$\Delta\epsilon_n = \frac{\bar{H}(k_p\sigma_r)}{\sqrt{45}}\frac{I_b}{I_A}(k_p L_b)^2(k_p L_{\mathrm{APL}}). \tag{17}$$

To validate the approximate expression of Eq. (17), the theoretical degradation is compared with modeling results obtained with the 2D-cylindrical particle-in-cell (PIC) code INF&RNO (using the quasi-static modality).[45,46] The following parameters, relevant to the LPA FEL application,[15] were used: $L_{\mathrm{APL}} = 2.9$ cm, $R_{\mathrm{APL}} = 500\,\mu$m, $\theta_0 = 1$ mrad, 250 MeV energy, $\epsilon_{n0} = 0.49\,\mu$m, $L_b = 2\,\mu$m, $I_b = 4.5$ kA (30 pC), $I_{\mathrm{APL}} = 750$ A, and $L_{\mathrm{drift}} = 9.3$ cm (thus $\sigma_r = 93\,\mu$m and beam density $n_{b0} = 1.7\times10^{15}\,\mathrm{cm}^{-3}$). One can observe in Fig. 5(b) that the emittance degradation both in the analytical expression and from the PIC code is strongly reduced at lower APL density $n_0 < 10^{17}\,\mathrm{cm}^{-3}$. The analytical expression Eq. (17) tends to overestimate the degradation by <20%, but otherwise good qualitative agreement was found. Through additional PIC studies, it was found that the emittance degradation was fairly insensitive to the choice of final (post-APL) drift length $L_{\mathrm{drift}}$. Also, the assumption of linear wakefields within the beam $-L_b \le \zeta \le 0$ was verified to be valid over the range of PIC simulations presented in Fig. 5.

A related parameter example is shown in Fig. 6, for three bunch durations $L_b = 1$, 2, and 3 $\mu$m. At 30 pC charge and size $\sigma_r = 93\,\mu$m, the beam densities are $n_{b0} = 3.5\times10^{15}$, $1.7\times10^{15}$, and $1.2\times10^{15}\,\mathrm{cm}^{-3}$, respectively. The linear dependence of the degradation on the bunch duration is revealed, due to the $I_b L_b^2$ term in Eq. (17) with $I_b \sim 1/L_b$. Note that while no lower limit on the APL density has been investigated or reported, it is speculated that at $H_2$ fill pressures below 1–2 Torr (electron densities below $n_0 < 10^{17}\,\mathrm{cm}^{-3}$), electrons from the capillary walls start to contribute to the plasma density inside the APL. This wall-ablation mechanism depends on various parameters such as the discharge current and APL radius and will limit the minimum near-axis plasma density that is achievable.

We now comment on the analytical wakefield-induced emittance growth based on the experimental conditions of Fig. 2, namely, an APL of length 1.5 cm, radius 500 $\mu$m, and density $10^{17}\,\mathrm{cm}^{-3}$, placed 24 cm from the source, and a

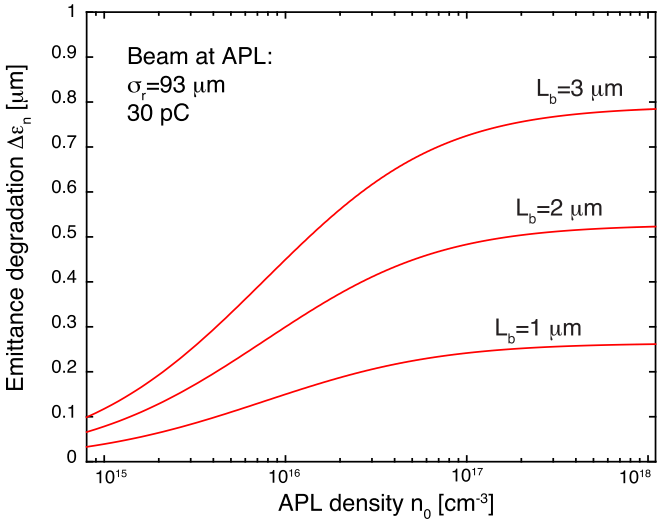


FIG. 6. Emittance degradation versus APL density $n_0$ keeping the charge fixed at 30 pC but varying the bunch duration at $L_b = 1$, 2, and 3 $\mu$m. Although the beam density decreases at larger $L_b$, the wakefield effects experienced by the tail electrons are enhanced due to the $\zeta^2$ scaling in $S(\zeta)$, leading to a larger emittance degradation.

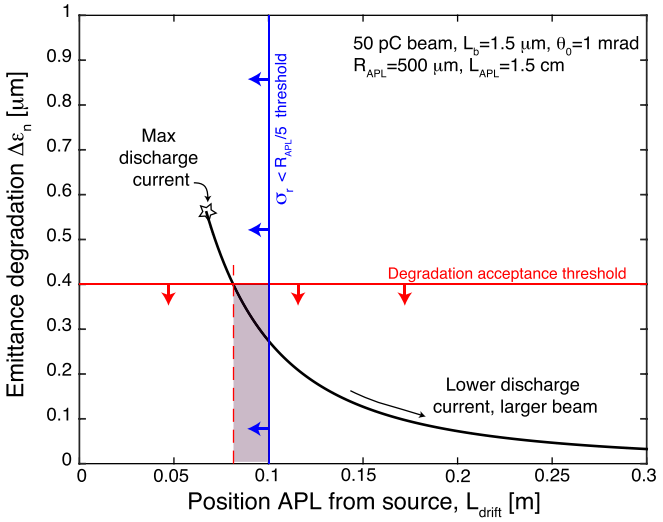


FIG. 7. APL. The black curve displays the emittance degradation from wakefield effects versus position $L_{\text{drift}}$ of the APL entrance from the source. Based on a maximum allowable degradation ($\Delta\epsilon_n = 0.4\,\mu$m here), a lower bound for $L_{\text{drift}}$ is set (vertical red dashed line). However, maintaining the condition $\sigma_r < R_{\text{APL}}/5$ derived from non-uniform discharge current considerations sets an upper bound on $L_{\text{drift}}$ (vertical solid blue line). The filled-in area displays the acceptable range of APL positions.

57 MeV electron beam of divergence 2.4 mrad, normalized emittance 1 $\mu$m, and charge 80 pC. With the bunch length unknown but estimated to be well below <15 fs, the emittance degradation varies from $\Delta\epsilon_n = 0.04\,\mu$m for $L_b = 1\,\mu$m to $\Delta\epsilon_n = 0.19\,\mu$m for $L_b = 5\,\mu$m, which is negligible when added in quadrature to the source emittance.

## V. DESIGN OF THE APL TRANSPORT LINE

The findings from the previously discussed two degradation mechanisms will be combined in an example design study (emittance degradation from non-uniform discharge currents favoring smaller beams and degradation from wakefields favoring larger beams). For this design, typical LPA source parameters were considered (200 MeV, 50 pC, $L_b = 1.5\,\mu$m, and $\theta_0 = 1$ mrad) and an APL with $R_{\text{APL}} = 500\,\mu$m and $L_{\text{APL}} = 1.5$ cm was selected to deliver focused beams to a plane 1 m from the LPA source. Only the position of the APL from the source (labeled $L_{\text{drift}}$) was used as a variable. At each position, the beam size at the entrance varies as $\sigma_r \approx \theta_0 L_{\text{drift}}$, and the discharge current was adjusted to maintain the imaging condition. The black curve in Fig. 7 displays the emittance degradation $\Delta\epsilon_n$ based on Eq. (17). The maximum achievable focusing gradient $(\partial B/\partial r)$, based on the limitations of the discharge pulser used, was chosen to be 710 T/m, which dictates the end of the curve (see star in Fig. 7). An "acceptance" degradation threshold of $\Delta\epsilon_n = 0.4\,\mu$m was defined, which provides a lower bound on the APL possible positions (see the area to the right of the vertical dashed red line). On the other hand, it was derived in Sec. III for sub-micron emittance beams that the beam size should satisfy $\sigma_r < R_{\text{APL}}/5$ to minimize emittance or charge density degradation associated with APL non-uniformity. This criterion adds an upper bound to the possible APL positions (see the area to the left of the solid blue line). Therefore, only a limited choice in the APL position remains, indicated by the filled-in area. For a $\epsilon_{n0} = 0.7\,\mu$m beam, the emittance degradation factor for drift distances in the 8–10 cm range is less than 15%. A similar design study will need to be performed for any selection of accelerator source and transport considerations.

## VI. CONCLUSION

In summary, we have experimentally compared a PMQ quadrupole triplet with an active plasma lens (APL) with a fixed LPA source and transport system, highlighting the reduced energy-dependence (chromaticity) in the APL-based transport line. The energy-resolved beam size measurements in both lens cases were similar, demonstrating no additional degradation in the APL. It is recognized, however, that the presence of transverse non-Gaussian wings in the beam even in the triplet case would have prevented observation of APL degradation effects discussed in this work.

Through transport simulations, the role of the non-uniformity of the radial discharge current distribution [and thus non-linear magnetic field profile $B(r)$] was investigated. Effectively, the electrons near the wall of the APL are pushed away from the core beam, leading to charge density and emittance degradation. For the 0.5 $\mu$m emittance considered, positioning a conceptual limiting aperture at the APL entrance of radius $R_{\text{aperture}} = R_{\text{APL}}/3$ minimizes the emittance degradation without further loss of charge density. Alternatively, the beam size should be $\sigma_r < R_{\text{APL}}/5$ to avoid degradation effects.

While APL current non-uniformity favors small beams, the fact that electrons inside the APL can be affected by self-driven wakefields favors a low beam density (larger beams). An analytical expression was derived for the beam-integrated emittance degradation, see Eq. (17). The degradation can be minimized for low APL densities $n_0 < 10^{17}\,\text{cm}^{-3}$, short capillaries, and larger beams. An example design study

was performed, showing that the emittance degradation can be kept below $\Delta\epsilon_n = 0.4\,\mu$m for a typical LPA source and transport line, including both degradation effects.

## ACKNOWLEDGMENTS

This work was supported by the U.S. Department of Energy (DOE) under Contract No. DE-AC02-05CH11231, by the National Science Foundation under Grant Nos. PHY-1415596 and PHY-1632796, by the U.S. DOE National Nuclear Security Administration, Defense Nuclear Nonproliferation R&D (NA22), and by the Gordon & Betty Moore Foundation under Grant ID GBMF4898.

[1]E. Esarey, C. B. Schroeder, and W. P. Leemans, Rev. Mod. Phys. **81**, 1229 (2009).
[2]J. Faure, Y. Glinec, A. Pukhov, S. Kiselev, S. Gordienko, E. Lefebvre, J.-P. Rousseau, F. Burgy, and V. Malka, Nature **431**(7008), 541 (2004).
[3]C. G. R. Geddes, C. Toth, J. van Tilborg, E. Esarey, C. B. Schroeder, D. Bruhwiler, C. Nieter, J. Cary, and W. P. Leemans, Nature **431**(7008), 538 (2004).
[4]S. P. D. Mangles, C. D. Murphy, Z. Najmudin, A. G. R. Thomas, J. L. Collier, A. E. Dangor, E. J. Divall, P. S. Foster, J. G. Gallacher, C. J. Hooker *et al.*, Nature **431**(7008), 535 (2004).
[5]W. P. Leemans, B. Nagler, A. J. Gonsalves, C. Tóth, K. Nakamura, C. G. R. Geddes, E. Esarey, C. B. Schroeder, and S. M. Hooker, Nat. Phys. **2**, 696 (2006).
[6]H. T. Kim, K. H. Pae, H. J. Cha, J. Kim, T. J. Yu, J. H. Sung, S. K. Lee, T. M. Jeong, and J. Lee, Phys. Rev. Lett. **111**, 165002 (2013).
[7]X. Wang, R. Zgadzaj, N. Fazel, Z. Li, S. A. Yi, X. Zhang, W. Henderson, Y.-Y. Chang, R. Korzekwa, H.-E. Tsai, and C.-H. Pai *et al.*, Nat. Commun. **4**, 1988 (2013).
[8]W. P. Leemans, A. Gonsalves, H.-S. Mao, K. Nakamura, C. Benedetti, C. Schroeder, C. Tóth, J. Daniels, D. Mittelberger, S. Bulanov *et al.*, Phys. Rev. Lett. **113**, 245002 (2014).
[9]W. T. Wang, W. T. Li, J. S. Liu, Z. J. Zhang, R. Qi, C. H. Yu, J. Q. Liu, M. Fang, Z. Y. Qin, C. Wang *et al.*, Phys. Rev. Lett. **117**, 124801 (2016).
[10]I. Tudosa, C. Stamm, A. B. Kashuba, F. King, H. C. Siegmann, J. Stöhr, G. Ju, B. Lu, and D. Weller, Nature **428**, 831 (2004).
[11]A. R. Maier, A. Meseck, S. Reiche, C. B. Schroeder, T. Seggebrock, and F. Grüner, Phys. Rev. X **2**, 031019 (2012).
[12]Z. Huang, Y. Ding, and C. B. Schroeder, Phys. Rev. Lett. **109**, 204801 (2012).
[13]C. B. Schroeder, E. Esarey, W. Leemans, and J. van Tilborg, see www.JACoW.org for Proceedings of FEL 2013 (JACoW, 2013).
[14]M. E. Couprie, A. Loulergue, M. Labat, R. Lehe, and V. Malka, J. Phys. B: At. Mol. Opt. Phys. **47**, 234001 (2014).
[15]J. van Tilborg, S. K. Barber, F. Isono, C. B. Schroeder, E. Esarey, and W. P. Leemans, AIP Conf. Proc. **1812**, 020002 (2017).
[16]Y. Glinec, J. Faure, L. L. Dain, S. Darbon, T. Hosokai, J. J. Santos, E. Lefebvre, J. P. Rousseau, F. Burgy, B. Mercier *et al.*, Phys. Rev. Lett. **94**, 025003 (2005).
[17]S. Chen, N. D. Powers, I. Ghebregziabher, C. M. Maharjan, C. Liu, G. Golovin, S. Banerjee, J. Zhang, N. Cunningham, A. Moorti *et al.*, Phys. Rev. Lett. **110**, 155003 (2013).
[18]N. D. Powers, I. Ghebregziabher, G. Golovin, C. Liu, S. Chen, S. Banerjee, J. Zhang, and D. P. Umstadter, Nat. Photonics **8**, 28 (2014).
[19]S. G. Rykovanov, C. Geddes, J.-L. Vay, C. Schroeder, E. Esarey, and W. Leemans, J. Phys. B: At. Mol. Opt. Phys. **47**, 234013 (2014).
[20]W. P. Leemans and E. Esarey, Phys. Today **62**(3), 44 (2009).
[21]S. Steinke, J. van Tilborg, C. Benedetti, C. G. R. Geddes, C. B. Schroeder, J. Daniels, K. K. Swanson, A. J. Gonsalves, K. Nakamura, B. H. Shaw *et al.*, Nature **530**, 190 (2016).
[22]B. Hidding, G. Pretzler, J. B. Rosenzweig, T. Königstein, D. Schiller, and D. L. Bruhwiler, Phys. Rev. Lett. **108**, 035001 (2012).
[23]E. Boggasch, J. Jacoby, H. Wahl, K. Dietrich, D. H. H. Hoffmann, W. Laux, M. Elfers, C. R. Haas, V. P. Dubenkov, and A. A. Golubev, Phys. Rev. Lett. **66**(13), 1705 (1991).
[24]B. Autin, H. Riege, E. Boggasch, K. Frank, L. D. Menna, and G. Miano, IEEE Trans. Plasma Sci. **15**, 226 (1987).
[25]F. Dothan, H. Riege, E. Boggasch, and K. Frank, J. Appl. Phys. **62**(9), 3585 (1987).
[26]A. A. Drozdovskii, A. A. Golubev, B. Y. Sharkov, S. A. Drozdovskii, A. P. Kuznetsov, Y. B. Novozhilov, P. V. Sasorov, S. M. Savin, and V. V. Yanenko, Phys. Part. Nucl. Lett. **7**, 534 (2010).
[27]J. van Tilborg, S. Steinke, C. G. R. Geddes, N. H. Matlis, B. S. Shaw, A. J. Gonsalves, J. V. Huijts, K. Nakamura, J. Daniels, C. B. Schroeder *et al.*, Phys. Rev. Lett. **115**, 184802 (2015).
[28]D. J. Spence and S. M. Hooker, Phys. Rev. E **63**(1), 015401 (2000).
[29]A. Butler, D. J. Spence, and S. M. Hooker, Phys. Rev. Lett. **89**(18), 185003 (2002).
[30]C. McGuffey, M. Levin, T. Matsuoka, V. Chvykov, G. Kalintchenko, P. Rousseau, V. Yanovsky, A. Zigler, A. Maksimchuk, and K. Krushelnick, Phys. Plasmas **16**, 113105 (2009).
[31]A. J. Gonsalves, F. Liu, N. A. Bobrova, P. V. Sasorov, C. Pieronek, J. Daniels, S. Antipov, J. E. Butler, S. S. Bulanov, W. L. Waldron *et al.*, J. Appl. Phys. **119**, 033302 (2016).
[32]J. van Tilborg, S. K. Barber, H.-E. Tsai, K. K. Swanson, S. Steinke, C. G. R. Geddes, A. J. Gonsalves, C. B. Schroeder, E. Esarey, S. S. Bulanov *et al.*, Phys. Rev. Accel. Beams **20**, 032803 (2017).
[33]R. Pompili, M. P. Anania, M. Bellaveglia, A. Biagioni, S. Bini, F. Bisesto, E. Brentegani, G. Castorina, E. Chiadroni, A. Cianchi *et al.*, Appl. Phys. Lett. **110**, 104101 (2017).
[34]N. A. Bobrova, A. A. Esaulov, J. Sakai, P. V. Sasorov, D. J. Spence, A. Butler, S. M. Hooker, and S. V. Bulanov, Phys. Rev. E **65**(1), 016407 (2001).
[35]S. K. Barber, C. B. Schroeder, J. van Tilborg, and W. P. Leemans, AIP Conf. Proc. **1812**, 040006 (2017).
[36]K. Swanson, H.-E. Tsai, S. Barber, R. Lehe, H.-S. Mao, S. Steinke, J. van Tilborg, K. Nakamura, C. Geddes, C. Schroeder *et al.*, Phys. Rev. Accel. Beams **20**, 051301 (2017).
[37]S. Bulanov, N. Naumova, F. Pegoraro, and J. Sakai, Phys. Rev. E **58**(5), R5257 (1998).
[38]C. G. R. Geddes, K. Nakamura, G. R. Plateau, C. Tóth, E. Cormier-Michel, E. Esarey, C. B. Schroeder, J. R. Cary, and W. P. Leemans, Phys. Rev. Lett. **100**(21), 215004 (2008).
[39]K. Schmid, A. Buck, C. M. S. Sears, J. M. Mikhailova, R. Tautz, D. Herrmann, M. Geissler, F. Krausz, and L. Veisz, Phys. Rev. ST Accel. Beams **13**(9), 091301 (2010).
[40]A. J. Gonsalves, K. Nakamura, C. Lin, D. Panasenko, S. Shiraishi, T. Sokollik, C. Benedetti, C. B. Schroeder, C. G. R. Geddes, J. van Tilborg *et al.*, Nat. Phys. **7**, 862 (2011).
[41]A. Buck, J. Wenz, J. Xu, K. Khrennikov, K. Schmid, M. Heigoldt, J. M. Mikhailova, M. Geissler, B. Shen, F. Krausz *et al.*, Phys. Rev. Lett. **110**, 185006 (2013).
[42]M. Fedurin, M. Babzien, V. Yakimenko, B. Allen, P. Muggli, and A. Murokh, in *Proceedings of the International Particle Accelerator Conference (IPAC'12, New Orleans), paper MOP057* (2012), p. 2753.
[43]S. K. Barber, J. van Tilborg, C. B. Schroeder, R. Lehe, H.-E. Tsai, K. K. Swanson, S. Steinke, K. Nakamura, C. G. R. Geddes, C. Benedetti *et al.*, Phys. Rev. Lett. **119**, 104801 (2017).
[44]S. K. Barber, J. van Tilborg, C. B. Schroeder, R. Lehe, H.-E. Tsai, K. K. Swanson, S. Steinke, K. Nakamura, C. G. R. Geddes, C. Benedetti *et al.*, "Parametric emittance measurements of electron beams produced by a laser plasma accelerator," Plasma Phys. Controlled Fusion (submitted).
[45]C. Benedetti, C. B. Schroeder, E. Esarey, C. G. R. Geddes, and W. P. Leemans, AIP Conf. Proc. **1299**, 250 (2010).
[46]C. Benedetti, C. Schroeder, C. Geddes, E. Esarey, and W. Leemans, Plasma Phys. Controlled Fusion **60**, 014002 (2018).